Published in Journal of Colloid and Interface Science 166, issue 2, 451-461, 1994
which should be used for any reference to this work

Determination of the Surface Fractal Dimension of Active Carbons by Mercury Porosimetry

FRANÇOISE EHRBURGER-DOLLE,*,[1] ANDRÉ LAVANCHY,† AND FRITZ STOECKLI‡

*Centre de Recherches sur la Physico-Chimie des Surfaces Solides, CNRS, 24 Avenue du Président Kennedy, F-68200 Mulhouse, France; †AC-Laboratorium, CH-3700 Spiez, Switzerland; and ‡Institut de Chimie, Université de Neuchâtel, 51 Avenue de Bellevaux, CH-2000 Neuchâtel, Switzerland

Mercury porosimetry has been used to characterize the macroporosity of several carbon materials activated by steam or carbon dioxide and their surface fractal dimension is determined. The first part is devoted to the analysis of the differential volume versus pressure curves in order to distinguish between mechanical effects resulting from the mercury pressure and true pore filling. It is shown, in the second part, that the macropore volume is not strongly affected by the activation process, but it depends mainly on the initial texture of the carbon. On the other hand, the fractal dimension varies largely with the activation conditions and burn-off. The experimental results suggest that the fractal dimension tends to increase with the degree of burn-off in steam, whereas the opposite occurs during activation by carbon dioxide. These observations are discussed in relation to the mechanisms of activation.

INTRODUCTION

Active carbons (1) are mostly used as adsorbents, catalysts, or catalyst supports, which means that they are concerned with phenomena occurring on the molecular scale. Therefore, active carbons are generally characterized by their morphology on the molecular scale, such as the surface area, volume, and width of the micropores (width < 2 nm) (2). The microporosity reflects the capacity to adsorb small molecules, such as common gases or solvent vapors. The adsorption of larger molecules will occur in larger pores, mesopores (2), of radii ranging between 1 and 25 nm and contributing mostly to the extent of the external surface area. The role of volume of macropores (pore radius > 25 nm) (2) seems to be limited to the transport of the gas molecules to be trapped in the micro- or mesopores. However, macropores are of great importance for some applications (3), as in nuclear industry or with respect to bacterial colonization, which may be requested in waste water cleaning or unacceptable in the purification of drinking water.

The classical method for the study of macropore size distribution is mercury porosimetry (4). The pore radius R is related to the mercury pressure P through the Whashburn equation

$$R \propto P^{-1}, \qquad [1a]$$

in which the prefactor is a function of the pore shape, the contact angle θ between the mercury and the surface of the solid, and the surface tension γ. The necessity to postulate a pore shape, the lack of reproducibility of the value of θ, and the fact that γ depends on the physical and chemical states of the solid surface (4) lead to an uncertainty on the value of the prefactor and, therefrom, on the value of R. In the following, we will show how the characterization of meso- and macropore geometry by means of the surface fractal dimension will overcome the above problems. However, as a first approximation, a cylindrical pore shape may be assumed. Thus,

$$R = -(2\gamma \cos\theta)/P. \qquad [1b]$$

With $\gamma = 0.48$ N/m and $\theta = 141.3°$, the usual equation is obtained,

$$R = 750/P, \qquad [1c]$$

in which R is expressed in nanometers and P in megapascals.

The second problem arising in mercury porosimetry is the effect of the pressure, which may lead to artifacts in the pore size distribution (PSD) curve (4) evaluated by means of Eq. [1c]. In the low-pressure range, compaction of the powder particles and/or filling of the interparticle voids may be interpreted as pores within the particles. At high pressures, mechanical breaking may occur, depending on the strength of the sample. Moreover, as shown by Kadlec (5), an inverse filling of supermicropores (i.e., supermicropores are filled at pressure lower than that required to fill mesopores) occurs when supermicropores are directly connected to macropores (for example, if they start on the walls of the macropores). This effect, however, is not possible when supermicropores

[1] To whom correspondence should be addressed.

are connected to macropores through mesopores. Therefore, it will be necessary to select the range of pressure corresponding to the filling of the macropores of the samples under investigation.

The benefit of using fractal geometry to evaluate the space-filling character (i.e., the pore size distribution) of solid surfaces was pointed out about 10 years ago by Pfeifer and Avnir (6) and it is widely used in the field of surface physics and chemistry (7). These authors have shown that the pore size distribution, dV/dR, is related to the surface fractal dimension D by means of the scaling law

$$-dV/dR \propto R^{2-D}. \quad [2]$$

As mentioned above, mercury porosimetry data result from the measurement of the intruded volume as a function of the applied pressure. From Eqs. [1a] and [2], it follows that

$$dV/dP \propto P^{D-4}. \quad [3]$$

Friesen and Mikula (8) have pointed out the benefit of using Eq. [3] to determine the fractal dimension from the mercury intrusion data. Formally, Eq. [3] is similar to Eq. [2], but in this case no assumption of the value of the prefactor in an R versus P relation is needed. Moreover, since by definition $2 < D < 3$, the scaling exponent in Eq. [3] lies between -2 and -1 in the case of fractal surfaces. Thus, if the experimental data fit with a power law with an exponent ranging between -1 and 0, the volume versus pressure data correspond no longer to volume filling of pores but describe the mechanical behavior of the sample (8, 9). A steeper slope would suggest the existence of a nonfractal, monodispersed porosity. Therefore, the study of the scaling exponent in different pressure domains will lead to the determination of the true domain of filling of the intraparticulate pores to be investigated as well as the actual macropore volume. This analysis will be presented in the first part of the paper.

The method proposed by Friesen and Mikula (8) has been applied to the characterization of coals (8, 9), chars (8), and coke particles (10) and to the investigation of the effect of oxidation by O_2 of a glassy carbon matrix in Coat-Mix materials (11) or of the combustion rate of coal chars (12) on the fractal dimension.

Mercury porosimetry has been widely used to determine the volume of pores ranging between 7500 and 3.75 nm (i.e., in the classical range of pore sizes expected with pressure ranging from 0.1 to 200 MPa), in the study of the overall porosity of active carbons (3, 13–16). However, the likelihood of the artifacts discussed above has never been examined. To our knowledge, the use of mercury porosimetry to determine the surface fractal dimension of active carbons, in the range of a few tens and a few hundreds of nanometers, has not yet been attempted.

The aim of the present paper is the investigation of the effect of the origin of the carbon material and the mode of activation (by steam or by carbon dioxide) on the value of the surface fractal dimension. The results will be correlated with the geometrical properties of the material, at the molecular scale, and with the mechanism involved in the oxidation process.

EXPERIMENTAL

Samples

With the exception of sample U-03, a steam-activated coal of industrial origin (Chemviron, Belgium), all solids were prepared from different precursors. These were subjected to similar treatments, described in detail elsewhere (17). The carbons resulted from Irish peat (TIM), coffee-bean skins (CAF), and a barbecue charcoal (CEP) obtained from soft wood.

The dry precursors TIM and CAF were first pyrolyzed for 2 h at 600°C under nitrogen and the light fractions were distilled off. Typical yields were around 35 and 20%, respectively. Subsequently, the solids were crushed and sieved (0.6 to 1.7 mm) and carbonized for 1 h at 850°C under nitrogen. At this stage, the weight losses were 20% (TIM) and 10% (CAF), but sample CEP, also subjected to this treatment, lost only a small percentage of its weight. These samples are referred as TIM-0, CAF-0, and CEP-0, respectively.

To produce the active carbons, the solids TIM-0, CAF-0, and CEP-0 were treated in batches of 10 g, with either steam or CO_2 at 850–900°C, as described earlier (17). These gases were carried by nitrogen and activation lasted usually between 60 and 240 min. The degree of activation (burn-off) is expressed by the relative weight loss of the carbonized material. It varied from 12 to 64%.

The structural properties of the carbons were determined by using standard adsorption and calorimetric techniques. On the basis of Dubinin's theory and its extensions (1, 17–19), it is possible to obtain information on the micropore volume V_{micro}, the so-called characteristic energy E_0, which is related to the average micropore width L, and the surface area S_{ext} located outside the micropores (it correspond to the walls of pores wider than 2 nm, approximately). The surface of the walls of the micropores, S_{micro}, can be estimated by assuming that micropores are slit shaped ($S_{micro} = 2 \times 10^3 V_{micro}/L$). This information is summarized in Table 1.

Mercury Porosimetry

The mercury porosimetry measurements were carried out with a Porosimeter 2000 (Carlo Erba). The mercury pressure P and intruded volume $V(P)$ were automatically increased, at a low speed, and the data were recorded. The maximum pressure is 194 MPa. The amount of sample ranged between

TABLE 1
Microporous Characteristics and External Surface Area of the Active Carbon Samples

Sample	V_{micro} (cm^3/g)	E_0 (kJ/mol)	L (nm)	S_{micro} (m^2/g)	S_{ext} (m^2/g)
U-03	0.519	17.2	1.9	550	62
TIM/W 12%	0.144	26.6	0.7	410	76
TIM/W 48%	0.176	24.9	0.8	440	250
CAF/W 14%	0.174	33.5	0.5	700	30
CAF/W 64%	0.455	20.7	1.2	750	213
CEP-0	0.157	37	0.4	790	29
CEP/W 18%	0.251	32.4	0.5	860	88
CEP/W 64%	0.585	24.5	0.8	1460	43
CEP/CD1 18%	0.250	33.3	0.5	860	59
CEP/CD1 57%	0.381	28.2	0.6	1270	33
CEP/CD2 18%	0.400	26.0	0.7	1140	6
CEP/CD2 42%	0.660	23.5	0.9	1470	10

0.15 and 0.35 g. The samples were outgassed at temperatures between 120 and 140°C under vacuum ($P < 500$ Pa) for 12 h before the measurements.

The radius R of the pores is calculated by means of Eq. [1c]. The volume $V(P)$ was corrected in order to take into account the compressibility of mercury in the high-pressure range. The resolution of the pressure value is 10^{-3} MPa and that of the intruded volume of mercury is 0.01 mm^3/g. It follows that the number of experimental points is large, particularly in the low-pressure region (small pressure increments) and in the upper-pressure range (small volume increments), leading to a large scattering of the dV/dP or dV/dR data. The effect of the minimum values of dP and dV on the precision of the regression lines was investigated and the values $(dP)_{min} = 0.05$ MPa and $(dV)_{min} = 0.5$ mm^3/g were selected.

ANALYSIS OF THE DATA

Principle of the Determination of the Fractal Dimension

For an object of fractal dimension D, the minimal number $N(R)$ of spheres of size R, needed to cover the whole object, varies as R^{-D} when R tends to zero (20). Then, if one equates the total volume of voids of sizes larger than R to the remaining volume of space when the object has been covered with these $N(R)$ spheres, one obtains

$$V(R) \propto \text{constant} - N(R)R^3 \propto \text{constant} - R^{3-D}, \quad [4]$$

from which the relation obtained by Pfeifer and Avnir (6) follows:

$$-dV/dR \propto R^{2-D}. \quad [2]$$

Therefore, Eq. [2] is directly related to the usual fractal scaling and D may be a mass or a surface fractal dimension (21). If D characterizes a mass fractal object with $D < 2$ (for example, cluster–cluster brownian aggregates), the slope of the PSD curve, plotted in logarithmic coordinates, is positive between the two cutoffs R_{min} and R_{max} (Fig. 1a). In the case of surface fractals, D is always larger than 2 and the slope of the PSD curve is negative, within the range of pore sizes (R_{min}, R_{max}) of the porous object (Fig. 1b). If $D = 2$, the slope is equal to zero and dV/dR is constant within the range R_{min}, R_{max}, as expected for a nonfractal surface. In the limiting case $R_{min} \approx R_{max}$, the shape of the curve becomes that of a narrow distribution of pore sizes, as shown in Fig. 1c, which is obviously not characteristic of a fractal surface. However, in some cases, one may observe a superposition of the curves in Figs. 1b and 1c, shown by the slope of the baseline, suggesting, for example, that the walls of such monodispersed pores are surface fractals or that the solid is heterogeneous.

It follows that a fractal surface will be characterized by an increasing volume of smaller and smaller pores. For a solid with a nonfractal surface ($D = 2$), although exhibiting a broad PSD curve, the volume of pores of decreasing sizes remains constant. On the other hand, mass fractals, such as aggregates with $D < 2$, are characterized by an increasing volume of larger and larger pores.

Analysis of the Different Domains of Pressure

In order to analyze the physical phenomena occurring over the whole range of pressures, three samples of carbon U-03 with different granulometries were investigated:

—The normal granulometry (U-03N) with grain sizes between 0.6 and 1.7 mm (12 × 30 mesh)

—A medium granulometry (sizes < 0.49 mm) (U-03M) obtained by a careful crushing of the normal grains and passing through a sieve of 0.49 mm opening (the small amount of dust inevitably formed during the crushing was not removed)

—A fine powder (U-03P) obtained after a stronger crushing and contained in the fraction passing through a sieve of 75 μm opening.

Figure 2a shows that, for all three samples, the dV/dP curves can be divided into three pressure domains:

—low-pressure range: $<0.1 < P < P_0$
—intermediate-pressure range: $P_0 < P < P_c$
—high-pressure range: $P > P_c$.

P_0 is close to 2 MPa and P_c is close to 50 MPa for normal (U-03N) and medium (U-03M) granulometry, whereas $P_c \approx 30$ MPa for the powder (U-03P).

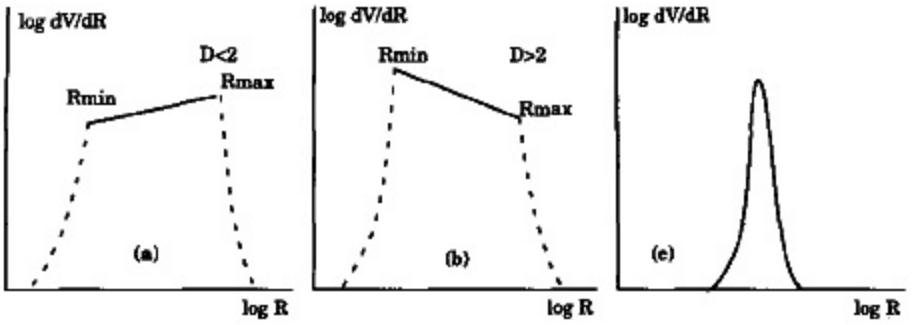

FIG. 1. Shape of a pore size distribution (PSD) curve expected for (a) a fractal aggregate with $D < 2$, (b) a fractal aggregate with $D > 2$ or a fractal surface, and (c) a nonfractal, narrow distribution.

Low-pressure range ($P < P_0$). The first step of the intrusion of a porous solid by mercury is the filling of the intergrain voids, which largely depends on the granulometry as also shown in Fig. 2a. If a random packing of uniform spheres of radius R_p is assumed, the solid volume fraction is close to 0.6 and the mean radius of the sphere inscribed in cavities is close to $0.53R_p$ (22). Therefore, the radius of the intergrain cavities would be found between 0.2 and 0.5 mm, below 130 μm, and below 20 μm, respectively, for the U-03N, U-03M, and U-03P samples. Obviously, this is a rough approximation giving an order of magnitude only, as we are dealing with mixtures of grain sizes and with random shapes, leading to more compact assemblies and/or smaller intergrain voids. In most cases, the peak of the dV/dP (or dV/dR) intergrain porosity curve is located below 0.1 MPa (i.e., above 7.5 μm) and the part of the curve measured in the low-pressure range corresponds to the decreasing left-hand side of the size distribution curve or to the right-hand side of the dV/dP versus P plots, tending to zero at complete filling of the intergrain voids (before the beginning of the filling of the pores within the grains). As there are no reasons for a fractal intergrain void size distribution (VSD), the slope of the curve is intuitively expected to be steep (Fig. 1c). In the case of the fine grains (sample P), the slope is larger than 2 (Fig. 2a), leading to a value of D smaller than 2. On the other hand, for coarse grains as in sample N, the slope is smaller than 1 and a value of D larger than 3 is obtained (Table 2). These results are also in agreement with those of Friesen and Mikula (8) for coal chars. While the results obtained for fine grains can be explained easily on the basis of the foregoing discussion, this is not the case for the coarse grains, for which the slope of the dV/dP curve is smaller than 1. A possible explanation could be proposed, if one assumes that a slope smaller than 1 reflects the mechanical behavior of the sample (similar to what occurs in the high-pressure range). In these circumstances, the increase in mer-

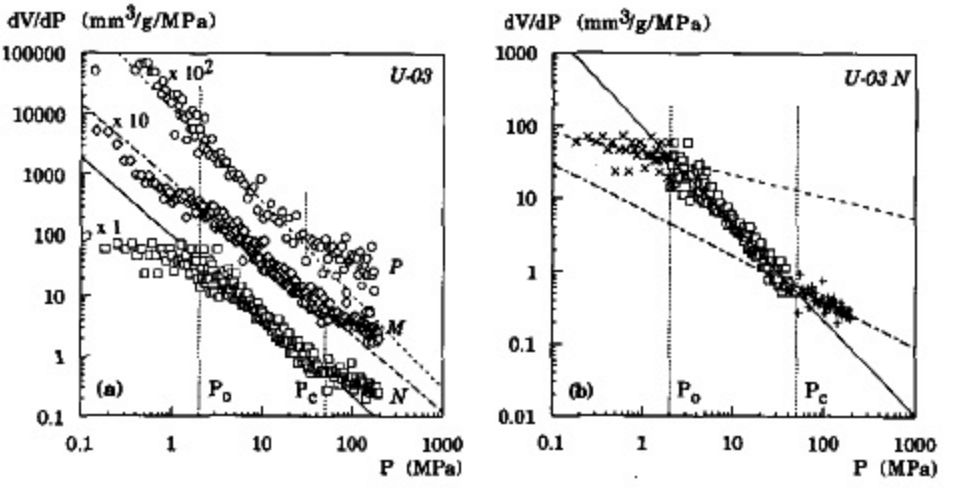

FIG. 2. dV/dP versus P curves obtained for U-03 samples: (a) Curves obtained for a normal granulometry (N), a mixture of grains of sizes <0.49 mm and powder (M), and a sample crushed into a fine powder (P). For the sake of clarity, the curves (M) and (P) have been shifted by a factor 10 and 10^2, respectively. (b) Curve dV/dP obtained for U-03 (normal granulometry) displaying the three different domains of pressure. The slopes of the fitting lines are indicated in Table 2.

TABLE 2

Values of the Slopes Obtained in the Different Pressure (or Corresponding Radius) Domains for U-03N (Normal Granulometry)

Range (P_0 = 2 MPa, P_c = 50 MPa)	Slope	D = 4 + (slope) (curve dV/dP)	D = 2 − (slope) (curve dV/dR)
P < 2 MPa	−0.29	"3.71"	
R > 375 nm	−1.60		"3.60"
2 < P < 50 MPa	−1.32	2.68	
15 < R < 375 nm	−0.68		2.68
P > 50 MPa	−0.63	"3.37"	
R < 15 nm	−1.35		"3.35"

cury pressure, once the intergrain voids are completely filled, could lead to the breaking of the largest and/or most irregularly shaped grains, by a mechanism similar to the one occurring in the dry powder, by attrition during shaking. Further developments and verification of this hypothesis would be interesting for a simple characterization of the mechanical strength of active carbons but are beyond the scope of the present paper.

Intermediate-pressure range ($P_0 < P < P_c$). The fractal dimension and the volume of macropores measured for samples U-03N with normal and U-03M with medium granulometry are very similar to each other but differ from those obtained for the powder sample U-03P (Table 3). It may be assumed that, in this case, there is a crossover between intrusion of mercury in the interparticle voids and macropore filling up to pressures larger than 2 MPa, leading to a larger slope and, therefore, to an apparently smaller fractal dimension. It is likely that the range of length corresponding to the macropores in these small particles is more narrow and can be hardly seen in the dV/dP curve. It is also possible that crushing leads to a smoothing of the surface due to the collapse of the overall macroporosity.

High-pressure range ($P > P_c$). In the high-pressure range, the behavior of the three samples is almost similar. Most authors (8–10) have assumed that the dV/dP curves measured above P_c reflect the compression or the breaking of the sample. One may also assume that the critical pressure P_c can be considered as the limit for mercury to fill pores, i.e., that the entrance of pores of sizes just below those filled at $P = P_c$ would be more narrow (constrictions). Obviously, in these circumstances, an increase in pressure will only lead to the deformation of the solid. It follows that P_c would determine the smallest pore size, R_{min}, directly accessible from the outside. Smaller pores, with radii $R \ll R_{min}$, may exist inside the material. This is suggested in some examples described below, by a peak in the dV/dP curve at $P \gg P_c$. However, at these pressures the mechanical deformation of the solid may also affect the remaining empty pores. It follows that the PSD curve obtained from the data measured above P_c may not correspond to the actual PSD in the initial material. Moreover, the pore size obtained in this pressure range may correspond to constrictions at the entrance of larger pores belonging to an internal mesoporous volume. It follows that the pressure range above P_c cannot be considered for the determination of a true pore size distribution.

From these observations, it may be concluded that only the intermediate-pressure range limited by P_0 and P_c can be used to investigate unambiguously the macropore region. These pressures are characteristics of the sample. Figures 3a and 3b show that the same results are obtained if the curves dV/dR versus R are considered, as expected from Eq. [2]. However, in this case, the quality of the fit is poorer. Therefore the true macropore region will be determined only from the location of the slope changes in the dV/dP versus P curves (i.e., P_0 and P_c) and the fractal dimension will be obtained from the slope of the fitting line in this pressure domain (in all cases, the values of r^2 are better than 0.90). However, in order to show the more familiar PSD curves, the results will also be shown in dV/dR versus R plots, by using the transformation of the data by means of Eq. [1c].

RESULTS

Evolution of Macroporosity and Surface Fractal Dimension during the Different Steps of Preparation of an Active Carbon (TIM Series)

The macroporosity of the pyrolyzed material (TIM pyrol.) extends over a large range of pore sizes (25–1500 nm) (Fig.

TABLE 3

Volume of Pores (in cm³/g) Determined in the Different Pressure Domains for U-03 and Surface Fractal Dimension

U-03	Normal (N) (0.6–1.7 mm)	Medium (M) (<0.49 mm + powder)	Powder (P) (<75 μm)
P_0 (MPa)	2	2	2
R_{max} (nm)	375	375	375
P_c (MPa)	50	50	30
R_{min} (nm)	15	15	25
V_{total} (cm³/g) (7500 < R < R_{min})	0.293	0.313	0.946
V_{inter} ($P < P_0$) ($R > R_{max}$)	0.091	0.121	0.775
V ($P > P_c$) ($R < R_{min}$)	0.054	0.052	0.056
V_{macro} ($P_0 < P < P_c$) ($R_{min} < R < R_{max}$)	0.148	0.140	0.115
Fractal dimension $D \pm 0.05$	2.68	2.73	2.46

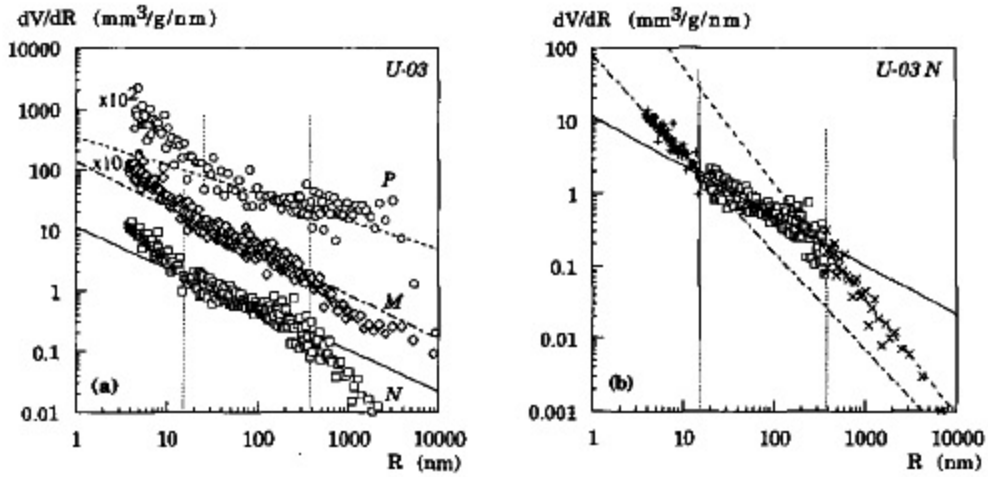

FIG. 3. (a, b) PSD curves obtained for U-03 samples, corresponding to the curves plotted in Figs. 2a and 2b, respectively.

4) and is characterized by a fractal dimension $D = 2.50$. The small volume (Table 4) measured for pressures below the change of slope at 0.5 MPa indicates that the intergrain porosity is filled by mercury at pressures smaller than 0.1 MPa. It follows that the interparticle voids and, therefore, the size of the grains are large. After carbonization at 850°C and before activation (TIM-0), the macropore volume (Table 4) is greatly reduced, owing to the disappearance of the largest pores (250 to 1500 nm) indicated by the higher value of P_0. The contribution of the smallest pores is less important (Fig. 4). Therefore the fractal dimension becomes much smaller ($D = 2.17$). Activation by steam leads to an increase in the fractal dimension, within the same range of pore sizes.

The value of P_c is the same for all samples. If P_c were related to the mechanical strength of the grains, one might expect a decrease in P_c with increasing burn-off as the result of a larger internal microporosity (Table 1). Since P_c remains constant, it can be assumed either that the mechanical strength remains constant up to 48% burn-off or that the radius R_{min} of the smallest accessible pore is unchanged. However, the increase of the nonmicroporous surface area, S_{ext} (Table 1), suggests an increase of the mesopore volume, i.e., the existence of smaller pores. This is confirmed by the peak located well below R_{min}. Therefore, it may be assumed that after steam activation of TIM to a 48% burn-off, the size of the mesopores remains either below 25 nm or accessible only through constrictions smaller than this value.

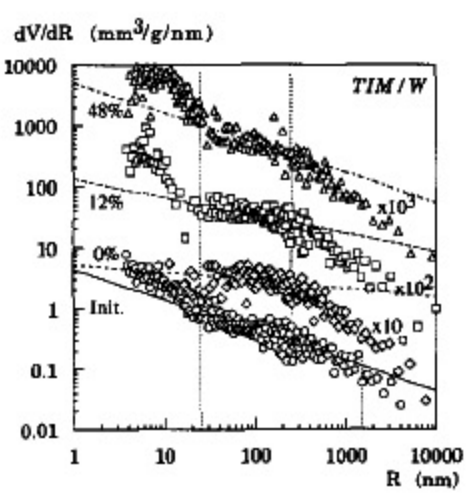

FIG. 4. PSD curves obtained for TIM samples.

CAF/W Series

The PSD curves obtained for CAF activated by steam to 14 and 64% are shown in Fig. 5. The surface fractal dimension (Table 4) increases with burn-off, whereas the range of macropore sizes becomes more narrow. For CAF/W 64%, the dV/dP curve shows a peak which can be attributed to macropores of sizes between 750 and 107 nm (Fig. 5). As the fractal dimension of this sample is still very high, it is likely that above a limiting burn-off (probably close to 50%), the oxidation leads to a partial collapse of pores, giving rise to larger macropores. As in the case of series TIM, the limiting pressure P_c remains constant. Therefore, the same conclusions are valid for this series.

CEP Series

Table 4 shows that the fractal dimension of the initial and unactivated solid is very high and it remains almost constant during activation by steam. The range of pore sizes is much larger than that for the previous samples (except the pyrolyzed, but not carbonized, sample TIM). Similarly to CAF/W 64%, CEP/W 64% exhibits a broad peak located between 200 and 2000 nm (Fig. 6). However, its origin may be dif-

TABLE 4
Experimental Results Obtained by Mercury Porosimetry on Active Carbons

Samples	V_{inter} (cm³/g)	P_0 (MPa)	P_c (MPa)	R_{max} (nm)	R_{min} (nm)	V_{macro} (cm³/g)	D (±0.05)
TIM pyrol.	0.194	0.5	30	1500	25	0.297	2.50
TIM-0	0.192	3	30	250	25	0.063	2.17
TIM/W 12%	0.204	3	30	250	25	0.073	2.29
TIM/W 48%	0.241	3	30	250	25	0.110	2.49
CAF/W 14%	0.117	3	20	250	37.5	0.066	2.28
CAF/W 64%	0.149	7	20	107	37.5	0.025	2.85
				750	*107*	*0.240*	*Peak*
CEP-0	0.205	0.5	10	1500	75	0.294	2.84
CEP/W 18%	0.519	0.5	10	1500	75	0.427	2.87
CEP/W 64%	0.670	0.5	70	150	11	0.283	2.86
				2000	*200*	*0.753*	*Peak*
CEP/CD1 18%	0.470	0.5	10	1500	75	0.346	2.60
CEP/CD1 57%	1.087	0.5	10	1500	75	0.444	2.10
CEP/CD2 18%	0.245	0.5	10	1500	75	0.321	2.70
CEP/CD2 42%	0.308	0.5	10	1500	75	0.371	2.64

Note. The uncertainty, estimated from the reproducibility of the data, is ±5%.

ferent. This question will be discussed below. Furthermore, for this series, P_c is much higher (P_c = 70 MPa) than that for all other samples. This suggests that down to 11 nm, the mesopores are accessible from the outside through larger pores, i.e., that there are no constrictions. In other words, the porosity ranging from 150 to 11 nm can be considered a surface porosity (and no longer an internal volume porosity). In contrast with the steam-activated CEP samples, the fractal dimension of the samples activated by carbon dioxide decreases with increasing burn-off (Table 4). The limit pressure, P_c, remains constant (P_c = 10 MPa). Therefore, as shown in Figs. 7a and 7b, the smallest pore size, R_{min}, remains relatively large (R_{min} = 75 nm). The comparison between the two series of CEP activated by CO_2 at 18% burn-off, for which the morphology at the molecular scale is different, as shown in Table 1, indicates that, also at the scale of the macropores, the texture is different. This question will be discussed below in more detail.

DISCUSSION

The experimental results given above have revealed considerable differences in the macroporosity of samples of dif-

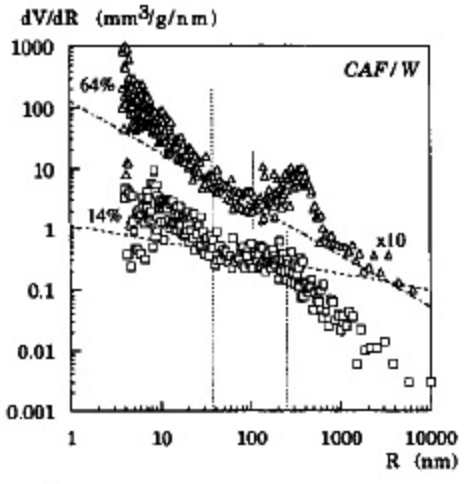

FIG. 5. PSD curves obtained for CAF samples.

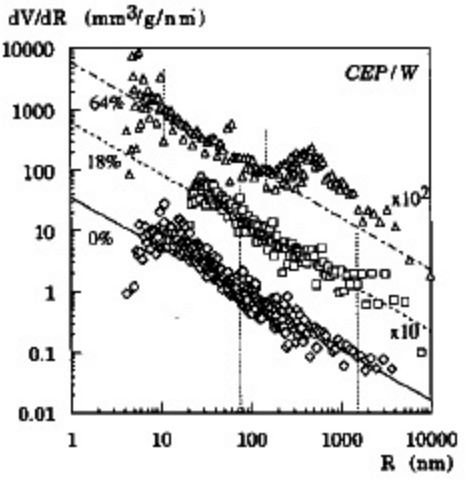

FIG. 6. PSD curves obtained for steam-activated CEP samples.

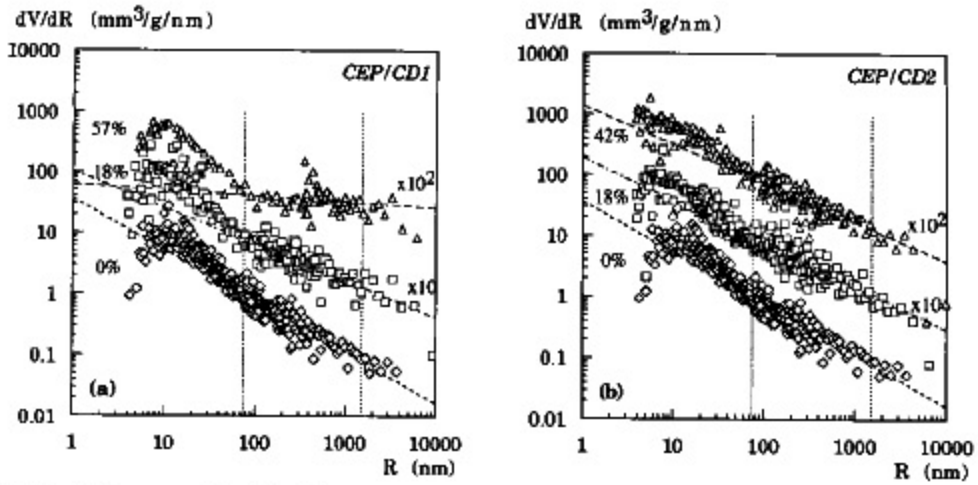

FIG. 7. PSD curves obtained for CEP samples activated by carbon dioxide: (a) series CD1 and (b) series CD2.

ferent origins, activation procedures, and burn-offs. In order to correlate these differences with the physical properties of the samples and the mechanism of activation, it is necessary to compare the pore volumes (micro, macro, and intergrain) of the samples by relating them to the *initial weight*, before oxidation of the carbon materials. The initial weight (in g[init]) is simply obtained by (1 + (burn-off)/100). Moreover, it might be interesting to compare the evolution of the pore volume, measured at different scales, with the theoretical volume of voids resulting from the loss of solid material by gasification, i.e., to convert the weight loss into a volume of voids. The density, d, of the solid material was determined by toluene pycnometry. A more or less constant value ($d \approx$ 2.07 g/cm^3) was obtained for all samples investigated. Obviously, the real density could be slightly larger, as a possible sealed-off microporosity is not taken into account. The values of the burn-off, expressed in volume of voids by g[init] and the different measured pore volumes, normalized to the initial mass of the sample, are collected in Table 5.

Evolution of the Size of the Grains with Activation

It was shown in the first part of this paper (Table 3) that the decrease of the size of U-03 grains leads to the increase of the measured intergrain volume. This apparently contradictory result is explained as follows. The initial size of the grains ranges between 0.6 and 1.7 mm. Therefore, the largest

TABLE 5

Summary of the Morphological Characteristics of the Different Active Carbons, Expressed by Unit Weight of Starting Carbon

Samples	$V_{burn\text{-}off}$ (cm^3/g[init])	V_{intr} (cm^3/g[init])	V_{macro} (cm^3/g[init])	D	V_{micro} (cm^3/g[init])	S_{micro} (m^2/g[init])	S_{ext} (m^2/g[init])
TIM-0	0	0.192	0.063	2.17			
TIM/W 12%	0.058	0.182	0.065	2.29	0.129	370	68
TIM/W 48%	0.230	0.163	0.074	2.49	0.119	300	169
CAF/W 14%	0.067	0.103	0.058	2.28	0.153	610	26
CAF/W 64%	0.307	0.091	0.015	2.85	0.277	460	130
			0.146	*Peak*			
CEP-0	0	0.205	0.294	2.84	0.157	790	29
CEP/W 18%	0.086	0.440	0.362	2.87	0.213	850	74
CEP/W 64%	0.307	0.409	0.173	2.86	0.357	890	26
			0.459	*Peak*			
CEP/CD1 18%	0.086	0.398	0.293	2.60	0.212	850	26
CEP/CD1 57%	0.274	0.692	0.283	2.10	0.243	810	19
CEP/CD2 18%	0.086	0.208	0.272	2.70	0.339	970	5
CEP/CD2 42%	0.202	0.217	0.261	2.64	0.465	1030	7

part of the intergrain void volume results from voids larger than the upper limit (7.5 μm) of the experimental method and, thus, cannot be measured. When the size of the grains decreases, the mean size of the voids decreases and a larger part of the void volume, located in voids smaller than 7.5 μm, can now be revealed by mercury porosimetry.

Similarly, an increase of the intergrain void volume in the active carbons investigated here will indicate a decrease of the grain size due to the activation process and/or to attrition effects resulting from a decrease of the mechanical strength. Table 5 indicates that, for TIM and CAF series, the intergrain void volume, i.e., the grain size, remains almost unchanged. Conversely, if one excepts CEP/CD2 samples, all samples of the CEP series exhibit a large increase of the intergrain void volume.

More information can be obtained from the comparison of the slopes of the dV/dP versus P lines in the low-pressure range ($0.1 < P < P_0$). In Fig. 8a we have plotted the curves obtained for two weakly steam-activated samples, CAF (a hard material) and CEP (a soft material). These plots can be compared with the ones (Fig. 2a) obtained for U-03N (normal granulometry) and U-03P (powder), respectively. For CAF/W 14%, the slope of the fitting line is also smaller than 1. This suggests, as already discussed in the case of U-03N, that this step corresponds to the breaking of grains already immersed in mercury, as the intergrain voids are filled at much lower pressures. Conversely, as in the case of U-03P, the slope obtained for CEP/W 18% is larger than 1. It follows that the grains of this softer material become smaller after breaking at a small mercury pressure, below 0.1 MPa, and that this step corresponds to the filling of the smallest intergrain voids.

After a stronger activation (64% burn-off), the PSD curves of both samples exhibit a peak located approximately between 200 and 1000 nm (Figs. 5 and 6). The dV/dP versus P curves (Fig. 8b) suggest that in the case of CAF, the peak corresponds to the filling of macropores resulting probably from the collapse of smaller pores during the activation process. Obviously this family of pores, exhibiting a symmetric distribution (Fig. 1c), does not correspond to a fractal surface. It is likely that such macropores also exist in CEP/W 64%. However, the extension of the process, characterized by a slope smaller than 1, up to 2 MPa, suggests the mechanical collapse and not the filling of such pores. It follows that, in this case, the corresponding PSD is meaningless. This example also enhances the importance of the study of the dV/dP versus P plots leading to the analysis of the different mechanisms involved during the mercury intrusion, in order to determine the range of pressure corresponding to a true macropore-filling process.

Evolution of the Macropore Volume with Activation

The volumes of macropores, measured between P_0 and P_c and normalized to the initial weight of sample, are collected in Table 5. This volume is systematically much larger in CEP samples than in TIM or CAF ones. This results mainly from the extent of the macroporosity up to macropores much larger (up to 1500 nm) in CEP samples than in the two other series (up to 200 nm), as shown in Figs. 9a and 9b.

If one excepts the case of CEP/W 18% characterized by a significant increase of the macropore volume and the two strongly activated samples (CEP/W 64% and CAF/W 64%), it may be concluded that the macropore volume is not strongly affected by the activation process. It can be considered, as a first approximation, as a characteristic of the initial texture of the carbon. Such a conclusion seems to be in contradiction with results obtained for active carbons prepared with almond shells or olive stones as precursors (23) but agrees with those reported for some other active carbons

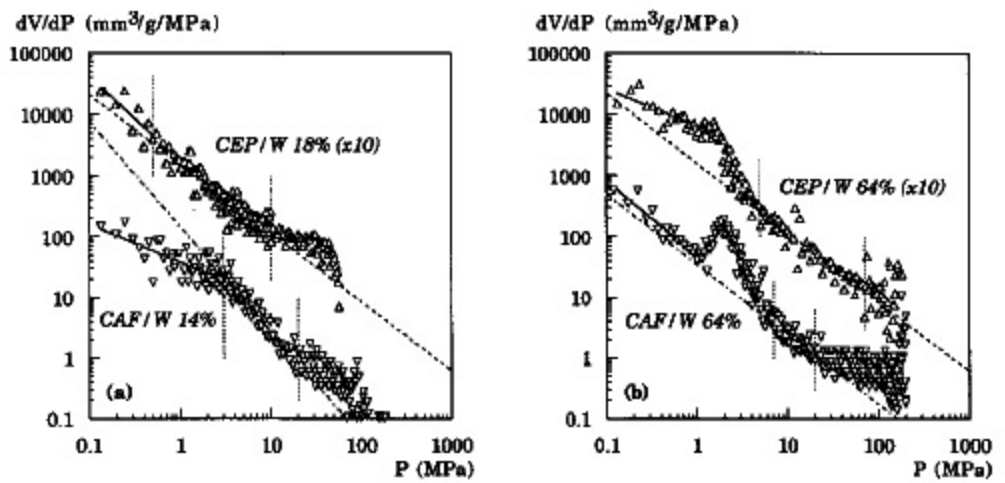

FIG. 8. Comparison of the dV/dP versus P plots obtained for steam-activated CAF and CEP: (a) at a low burn-off (<20%) and (b) at a high burn-off (64%).

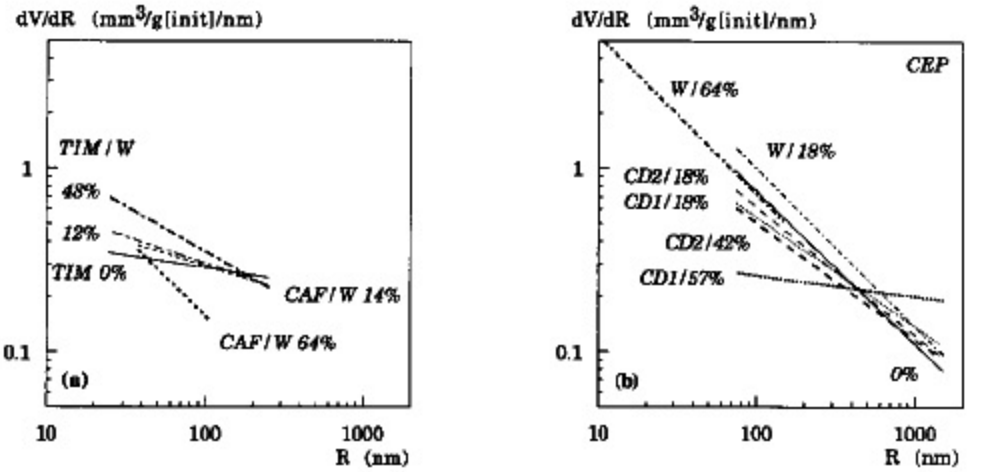

FIG. 9. (a, b) Evolution of the PSD curves, represented by the fitting lines, with burn-off for the different types of active carbon.

(24). However, it has to be noted that in all former papers, the value of the macropore volume was determined over the whole range of pore sizes, without taking into account some mechanical effects due to the mercury pressure.

Relation between the Evolution of the Fractal Dimension during Steam Activation and the Initial Texture of the Carbon Material

As indicated in Table 5, the fractal dimension of the non-activated TIM carbon (and likely also the CAF carbon) is small and increases with burn-off, whereas that of the CEP carbon is very high and remains similar at a low (18%) and high (64%) burn-off.

TIM and CAF carbons. Figure 9a shows that, for the TIM series, the increase of the fractal dimension during activation by steam at 12 and 48% burn-off results from an increasing contribution of pores of decreasing sizes. The micropores are slightly enlarged (Table 1), their volume slightly decreases (Table 5), and the surface of the walls decreases. Therefore, a part of the former micropores reaches the size of mesopores and contributes to the increase of S_{ext}. This result confirms that steam activation leads to an enlarging of micropores and to the shift to meso- and macropores (23).

It is likely that the same mechanism would be pertinent to CAF samples. However, in the case of the strongly activated CAF sample (CAF/W 64%), another effect occurs simultaneously. The high value of the fractal dimension results from the disparition of the largest pores as shown in Fig. 9a. This could result from the ablation of the external part of an increasingly corrugated surface, leading finally to the formation of large holes within the sample, as shown in Fig. 5.

CEP carbons. Figure 9b shows that the PSD curves obtained for CEP-0 and CEP/W 18% are similar but that the corresponding pore volume is increased (Table 5). Since the porosity ranging between 1500 and 75 nm is similar in the two samples, it is probably not involved in a reaction with steam. Since the corresponding volume is increased, it suggests that, in CEP-0, a fraction of this macroporosity is not accessible for mercury in the P_0, P_c pressure range. This could be attributed either to an initial sealing off by solid walls or to constrictions smaller than 75 nm. Actually, the reduction of the mechanical strength would support the first hypothesis.

The VSD curve obtained for CEP/W 64% is characterized by the disparition of the largest pores within the fractal structure, which is likely to proceed from the same mechanism as that already assumed for CAF/W 64% and by the extent of the same VSD curve as that obtained for the initial sample up to much smaller pores (11 nm). It follows that the surface of CEP samples is probably fractal over a very broad range of pore sizes (11 to 1500 nm) but that constrictions could be induced during the carbonization step.

In contrast with the two other series, the surface of the micropore walls increases. This could result either from a micropore deepening mechanism (which would be expected at a higher activation temperatures only (24)) occurring simultaneously with the micropore drilling or from the opening of a sealed-off microporosity. In such circumstances the increase of S_{ext} is probably not due to a shift of some enlarged micropores in the mesopore range. The opening of constricted mesopores would probably be a more realistic explanation.

Influence of the Activation Agent (Steam or Carbon Dioxide) on the Fractal Dimension of CEP Samples

Figure 9b shows that for both series of CO_2-activated samples, the contribution of the smaller pores decreases and that of the largest ones increases, leading to the diminution of

the fractal dimension (Table 5). It is interesting to note that CEP/W 18% and CEP/CD1 18% have the same microporous characteristics. This is in agreement with the general observation that, at low burn-offs, the reaction of carbon dioxide and steam in micropores is similar. However, as expected, the mechanism of oxidation of the external surface is very different. The lowering of D, corresponding to a smoothening of the surface, agrees with the expected effect of ablation of the external surface by CO_2, leading to a decrease of the grain sizes as suggested by the large value of the intergrain volume obtained for CEP/CD1 57%.

In the case of CEP/CD2 series, the fractal dimension remains larger than that for the former. Moreover, the increase of the micropore volume (0.18 and 0.31 cm^3/g after 18 and 42% burn-off, respectively) is much larger than the volume of carbon gasified, indicated in Table 5. It follows that, for this particular series, the increase of the micropore volume results mainly from the opening of constricted micropores. Simultaneously, the ablation of the external surface is reduced, limiting the decrease of the fractal dimension and that of the grain size. However, the drastic decrease of S_{ext} is difficult to explain.

Therefore, from the comparison between the evolution of the fractal dimension during steam or carbon dioxide activation, one may conclude, as intuitively expected, that the first process leads to an increase whereas the latter leads to a decrease of D. However, our experimental results suggest that the mechanism of oxidation by steam of a carbon characterized by a high D value could be different from that of carbon materials characterized by a low D value. Therefore, the above conclusion must be taken with some caution and more experimental work is necessary before it can be generalized to all systems.

CONCLUSION

The investigation of the porous texture of active carbons by mercury porosimetry leads to significant information concerning the morphology of the samples over a broad range of length scale. Particularly, this method reveals the important role of the initial texture of the carbon material, characterized by its surface fractal dimension, on the development of the porosity due to a given activation process. This could also induce further theoretical studies concerning the kinetics (7, 25) of the reactions of carbon dioxide or steam with a fractal surface of carbon.

Obviously, mercury porosimetry alone is not able to completely characterize the texture of the material, and classical adsorption methods and/or immersion calorimetry (1) must be used in order to investigate the surface of the solid at a molecular scale. Meanwhile, mercury porosimetry appears to be indispensable for a better approach of the mechanisms of activation, provided that the true macropore-filling process, leading to the PSD curve, is clearly separated from mechanical effects of the mercury pressure on the carbon material. In these circumstances, the determination of the two limiting pressures P_0 and P_c from the differential volume versus pressure plots (i.e., also the pore size range) and the fractal dimension D could be considered as "fingerprints" of a given type of active carbon and could be used to check the specifications of different batches of active carbons used for practical applications.

ACKNOWLEDGMENT

The authors thank Markus Stöckli (AC-Laboratorium Spiez) for performing the mercury porosimetry measurements.

REFERENCES

1. Bansal, R. C., Donnet, J. B., and Stoeckli, F., "Active Carbon." Dekker, New York, 1988.
2. Sing, K. S. W., Everett, D. H. R., Haul, A., Moscou, L., Pierotti, R. A., Rouquerol, J., and Siemieniewska, T., *Pure Appl. Chem.* **57**, 603 (1985).
3. Wildman, J., and Derbyshire, F., *Fuel* **70**, 655 (1991).
4. Gregg, S. J., and Sing, K. S. W., "Adsorption, Surface Area and Porosity," p. 173. Academic Press, London, 1982.
5. Kadlec, O., *Carbon* **27**, 141 (1989).
6. Pfeifer, P., and Avnir, D., *J. Chem. Phys.* **79**, 3558 (1983).
7. Farin, D., and Avnir, D., *in* "The Fractal Approach to Heterogeneous Chemistry" (D. Avnir, Ed.), p. 271. Wiley, Chichester, 1989.
8. Friesen, W. I., and Mikula, R. J., *J. Colloid Interface Sci.* **120**, 263 (1987).
9. Friesen, W. I., and Mikula, R. J., *Fuel* **67**, 1516 (1988).
10. Ng, S. H., Fairbridge, C., and Kaye, B. H., *Langmuir* **3**, 340 (1987).
11. Ehrburger-Dolle, F., Fox, T., Lahaye, J., and Luhleich, H., *in* "Carbone 90, Paris, 16–20 July 1990," p. 32. [Extended Abstract]
12. Salatino, P., Zimbardi, F., and Masi, S., *Carbon* **31**, 501 (1993).
13. Gonzalez-Vilchez, P., Linares-Solano, A., Lopez-Gonzalez, J. de D., and Rodriguez-Reinoso, F., *Carbon* **17**, 441 (1979).
14. Gomez-Serrano, V., Sanchez-Iniguez, F., and Valenzuela-Calahorro, C., *Fuel* **70**, 1083 (1991).
15. Mittelmeijer-Hazeleger, M. C., and Martin-Martinez, J. M., *Carbon* **30**, 695 (1992).
16. Domingo-Garcia, M., Fernandez-Morales, I., and Lopez-Garzon, F. J., *Carbon* **31**, 75 (1993).
17. Stoeckli, F., and Ballerini, L., *Fuel* **70**, 557 (1991).
18. Krähenbühl, F., Stoeckli, F., Addoun, A., Ehrburger, P., and Donnet, J. B., *Carbon* **24**, 483 (1986).
19. Stoeckli, F., and Krähenbühl, F., *Carbon* **22**, 297 (1984).
20. Pfeifer, P., and Obert, M., *in* "The Fractal Approach to Heterogeneous Chemistry" (D. Avnir, Ed.), p. 11. Wiley, Chichester, 1989.
21. Ehrburger-Dolle, F., Mors, P. M., and Jullien, R., *J. Colloid Interface Sci.* **147**, 192 (1991).
22. Avery, R. G., and Ramsay, J. D. F., *J. Colloid Interface Sci.* **42**, 597 (1973).
23. Rodriguez-Reinoso, F., *in* "Fundamental Issues in Control of Gasification Reactivity" (J. Lahaye and P. Ehrburger, Eds.), Vol. 192, p. 533. NATO ASI Series, Series E: Applied Sciences, Kluwer, Dordrecht, 1991.
24. Wigmans, T., *Carbon* **27**, 13 (1989).
25. Kopelman, R., *in* "The Fractal Approach to Heterogeneous Chemistry" (D. Avnir, Ed.), p. 295. Wiley, Chichester, 1989.